# The Structure of Dasatinib (BMS-354825) Bound to Activated ABL Kinase Domain Elucidates Its Inhibitory Activity against Imatinib-Resistant ABL Mutants

John S. Tokarski, John A. Newitt, Chieh Ying J. Chang, Janet D. Cheng, Michael Wittekind, Susan E. Kiefer, Kevin Kish, Francis Y.F. Lee, Robert Borzillerri, Louis J. Lombardo, Dianlin Xie, Yaqun Zhang, and Herbert E. Klei

Bristol-Myers Squibb Company, Pharmaceutical Research Institute, Princeton, New Jersey

## Abstract

**Chronic myeloid leukemia (CML) is caused by the constitutively activated tyrosine kinase breakpoint cluster (BCR)-ABL. Current frontline therapy for CML is imatinib, an inhibitor of BCR-ABL. Although imatinib has a high rate of clinical success in early phase CML, treatment resistance is problematic, particularly in later stages of the disease, and is frequently mediated by mutations in BCR-ABL. Dasatinib (BMS-354825) is a multitargeted tyrosine kinase inhibitor that targets oncogenic pathways and is a more potent inhibitor than imatinib against wild-type BCR-ABL. It has also shown preclinical activity against all but one of the imatinib-resistant BCR-ABL mutants tested to date. Analysis of the crystal structure of dasatinib-bound ABL kinase suggests that the increased binding affinity of dasatinib over imatinib is at least partially due to its ability to recognize multiple states of BCR-ABL. The structure also provides an explanation for the activity of dasatinib against imatinib-resistant BCR-ABL mutants.** (Cancer Res 2006; 66(11): 5790-7)

## Introduction

The Philadelphia chromosome is a result of translocation between human chromosomes 9 and 22 and fuses the *c-ABL* gene with the *breakpoint cluster* (*BCR*) gene (1). The resulting BCR-ABL fusion protein is a constitutively active, oncogenic tyrosine kinase that causes cell transformation and chronic myeloid leukemia (CML; ref. 2). BCR-ABL is also responsible for malignant transformation in 15% to 30% of patients with acute lymphoblastic leukemia (ALL; ref. 3). Imatinib (STI-571, Gleevec; Fig. 1*B*) has been established as frontline treatment for CML (4, 5). It is a drug that exerts its effect by binding to the ABL kinase domain and inhibiting the tyrosine kinase activity of BCR-ABL This results in a normalization of peripheral WBC counts and a substantial reduction of the Philadelphia chromosome-positive clone of stem cells in bone marrow, effectively offering hematologic and cytogenetic responses in the clinic. Although response rates to imatinib treatment are high in early (chronic phase) CML, responses in more advanced CML and ALL are only short lived (6–8). Furthermore, acquired resistance to imatinib represents a growing problem at all stages of CML, most often due to point mutations in BCR-ABL. Other mechanisms of resistance, both BCR-ABL dependent and BCR-ABL independent, such as overexpression of other tyrosine kinases, may also occur (9, 10).

Restoration of BCR-ABL-mediated signaling in the leukemic cells of patients with acquired imatinib resistance is due to point mutations in the ABL kinase domain in 70% to 90% of patients with CML (11). The structure of ABL kinase with imatinib [Protein Data Bank (PDB) ID 1IEP; ref. 12] reveals that these mutations occur either at residues directly implicated in imatinib binding or, more commonly, at residues important for the ability of the kinase to adopt a specific inactive conformation favorable to imatinib (11, 13). Dasatinib [*N*-(2-chloro-6-methylphenyl)-2-(6-(4-(2-hydroxyethyl)piperazin-1-yl)-2-methylpyrimidin-4-ylamino)thiazole-5-carboxamide; ref. 14; Fig. 1*A*] is a novel, orally available, small-molecule multitargeted kinase inhibitor that potently inhibits BCR-ABL and SRC family kinases and is 325-fold more potent than imatinib against cells expressing wild-type BCR-ABL (15).

Dasatinib also potently inhibits imatinib-resistant BCR-ABL mutants. In a previous study, dasatinib was tested against 15 clinically relevant imatinib-resistant BCR-ABL mutants using cell-based biochemical and biological assays; 14 of these mutants were effectively inhibited in the low nanomolar range (16). Importantly, all imatinib-resistant BCR-ABL mutations located in the phosphate-binding loop (P-loop) of ABL kinase, which have been associated with poor prognosis (17), were successfully targeted by dasatinib. Additionally, dasatinib blocked the kinase activity of imatinib-resistant BCR-ABL mutants where the mutations reside in the activation loop and other sites in the COOH-terminal lobe. The only imatinib-resistant BCR-ABL mutant that was resistant to dasatinib in this *in vitro* study was the T315I mutant. In addition to cellular assays, dasatinib has shown *in vivo* efficacy, with no apparent toxicity, when given orally to severe combined immunodeficient mice with established leukemias derived from i.v. injection of Ba/F3 cells expressing wild-type BCR-ABL or the most commonly encountered imatinib-resistant BCR-ABL mutants.

The ability of dasatinib to effectively inhibit the proliferation of cells expressing nearly all imatinib-resistant mutants tested to date suggests that this compound has significant therapeutic potential in the setting of imatinib-resistant CML. Indeed, a phase I dose escalating study has shown promising results in imatinib-resistant and imatinib-intolerant patients with all phases of CML and with Philadelphia chromosome-positive ALL (18). These phase I data are supported by preliminary results of four phase II trials in the

**Note:** J.D. Cheng and M. Wittekind are currently at Amgen, 1201 Amgen Court West, Seattle, WA 98119.

The authors are employed by Bristol-Myers Squibb. Dasatinib is currently in phase II clinical trials for the treatment of imatinib-resistant chronic myeloid leukemia and Philadelphia chromosome-positive acute lymphoblastic leukemia.

**Requests for reprints:** John S. Tokarski, Department of Structural Biology and Modeling, Bristol-Myers Squibb Pharmaceutical Research Institute, P.O. Box 4000, Princeton, NJ 08543. Phone: 609-252-6154; Fax: 609-252-6030; E-mail: john.tokarski@bms.com.



doi:10.1158/0008-5472.CAN-05-4187

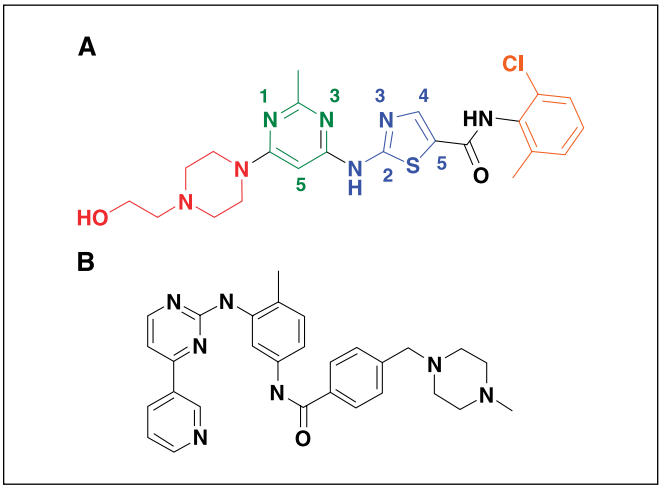


**Figure 1.** *A,* two-dimensional structure of dasatinib. The atom numbering within the pyrimidine and thiazole rings is provided for reference. *Red,* hydroxyethyl-piperazine group; *green,* pyrimidine group; *blue,* aminothiazole group; *black,* amide group; *orange,* 2-chloro-6-methyl phenyl group. *B,* two-dimensional structure of imatinib.

"START" (SRC/ABL Tyrosine kinase inhibition activity: Research Trials of dasatinib program), which have now closed (19–22). Further follow-up of patients in these phase II studies is ongoing.

Here, we report the crystal structure of the ABL kinase domain in complex with dasatinib. We undertook this study to provide a structural rationale for the mechanism of potent BCR-ABL inhibition by dasatinib and the favorable activity of dasatinib against imatinib-resistant mutants.

## Materials and Methods

**Construct design.** Forward (CGGCCATATGCACGACCGAAAACCTG-TATTTTCAGGGTGCCATGGATCCGTCCTCCCCCAACTACGACAAGTGGG) and reverse (GGCCGAATTCTTATTAGGTGCCACGTTTCCCCAGCTCCTTT-TCCACTTCG) primers were used to amplify the kinase domain from a cDNA encoding human c-ABL (HSABL, accession X16416) and create an insert with a 5′-*Nde*I site, a sequence encoding a tobacco etch virus (TEV) protease cleavage site, the kinase domain, and a 3′-*Eco*RI site. This fragment was inserted into the baculovirus transfer vector pAcHLT-A (BD Biosciences PharMingen, San Jose, CA) cut with *Nde*I and *Eco*RI to construct the vector ABL/pAcHLT-A, encoding a $NH_2$-terminal $(His)_6$ fusion protein under control of the polyhedrin promoter. Following expression, purification, and removal of the $(His)_6$ fusion protein tag with TEV protease, the encoded protein contained non-native residues GAMDPS at the $NH_2$ terminal, human c-ABL S229-K512 (accession CAA34438), and mouse c-ABL residues R513-T515 at the COOH terminal. This protein was identical to 1FPU (23), except for the serine to asparigine difference between the mouse and human sequences, respectively, at amino acid residue 336 in the human c-ABL sequence.

**Recombinant baculovirus production and protein expression.** ABL/pAcHLT-A was co-transfected with linearized baculovirus DNA (Baculo-Gold, BD Biosciences PharMingen) into Sf9 cells according to the manufacturer's protocol. A clonal population of recombinant virus was obtained by plaque purification. Recombinant virus was harvested and further amplified. Virus titer was determined using a standard plaque assay. After screening various variables, optimal conditions for $(His)_6$-ABL kinase protein expression were identified. Sf9 cells ($2 \times 10^6$ per mL) were grown in SF900-II medium in a Wave bioreactor (24). Recombinant baculovirus encoding $(His)_6$-ABL kinase was inoculated at a multiplicity of infection of five in the presence of 30% oxygen in the head space. Cells were harvested 72 hours after infection by centrifugation and frozen at −70°C. $(His)_6$-ABL kinase protein expression was estimated to be 5 mg/L of culture.

**Purification of ABL kinase domain and formulation with imatinib and dasatinib.** The ABL kinase domain was purified and combined with inhibitors as reported previously (12) with minor modifications. Frozen cell paste from baculovirus-infected Sf9 cells was thawed and resuspended in 10 volumes of lysis buffer [50 mmol/L Tris-HCl (pH 8), 20 mmol/L NaCl, 10% (v/v) glycerol, 10 mmol/L DTT, Complete EDTA-free protease inhibitor cocktail (Roche, Indianapolis, IN)]. Cells were lysed by cavitation after nitrogen pressurization to 450 p.s.i. for 30 minutes at 4°C. The lysate was clarified by sedimentation at 100,000 × $g_{max}$ for 40 minutes at 4°C. The supernatant was loaded onto a Q-Sepharose Fast Flow column equilibrated with 50 mmol/L Tris-HCl (pH 8), 20 mmol/L NaCl, 10% (v/v) glycerol, and 10 mmol/L DTT. The column was washed and eluted with a linear gradient of 20 to 500 mmol/L NaCl in 50 mmol/L Tris-HCl (pH 8), 10% (v/v) glycerol, and 15 mmol/L β-mercaptoethanol. $(His)_6$-ABL kinase was eluted in the gradient with 250 mmol/L NaCl and loaded onto a Ni-NTA Superflow (Qiagen, Valencia, CA) column equilibrated with 20 mmol/L imidazole. The column was eluted with a linear gradient of imidazole to 750 mmol/L. $(His)_6$-ABL kinase containing fractions were pooled and incubated at 50 μmol/L concentration at 4°C for 18 hours with 1 unit recombinant TEV (rTEV) protease (Invitrogen, Carlsbad, CA) per 3 μg protein to remove the $(His)_6$ affinity tag. A 3× molar excess (150 μmol/L) of either imatinib or dasatinib was added from 15 mmol/L DMSO stocks to the completed rTEV digest. The ABL kinase inhibitor complex was purified and exchanged into the final buffer by chromatography on a Superdex 75 column in 20 mmol/L Tris-HCl (pH 8), 100 mmol/L NaCl, and 3 mmol/L DTT. The final yield of purified ABL kinase protein was ~2.7 mg/L of culture. Purified ABL kinase inhibitor complexes were concentrated to 5 or 10 mg/mL with Amicon-ultra 10,000 molecular weight cut-off centrifugal ultrafilters (Millipore, Billerica, MA) before crystallization.

**Table 1.** Data collection and refinement statistics

| | ABL-dasatinib* |
|---|---|
| Data collection | |
| Space group | $P4_32_12$ |
| Unit cell variables | |
| *a, b, c* (Å) | 105.2, 105.2, 111.1 |
| *α, β, γ* (°) | 90, 90, 90 |
| Resolution range (Å) | 50-2.4 (2.49-2.4) |
| $R_{sym}$ (%) | 12.7 (50.9) |
| Average I/σ (I) | 17.1 (4.5) |
| Completeness (%) | 100 (100) |
| Number of observations | 187,605 (18,658) |
| Number of unique reflections | 25,102 (2,455) |
| Average redundancy | 7.5 (7.6) |
| Refinement | |
| Resolution range (Å) | 50-2.4 |
| Number of reflections | 24,996 |
| $R_{work}/R_{free}$ (%) | 21.9/28 |
| Number of atoms | |
| Protein | 4,518 |
| Ligand/ion | 66 |
| Water | 315 |
| RMS deviations | |
| Bond lengths (Å) | 0.006 |
| Bond angles (°) | 1.4 |

*Data were collected from one cryomounted crystal. No visible decay of the diffraction pattern was observed over the course of the experiment.

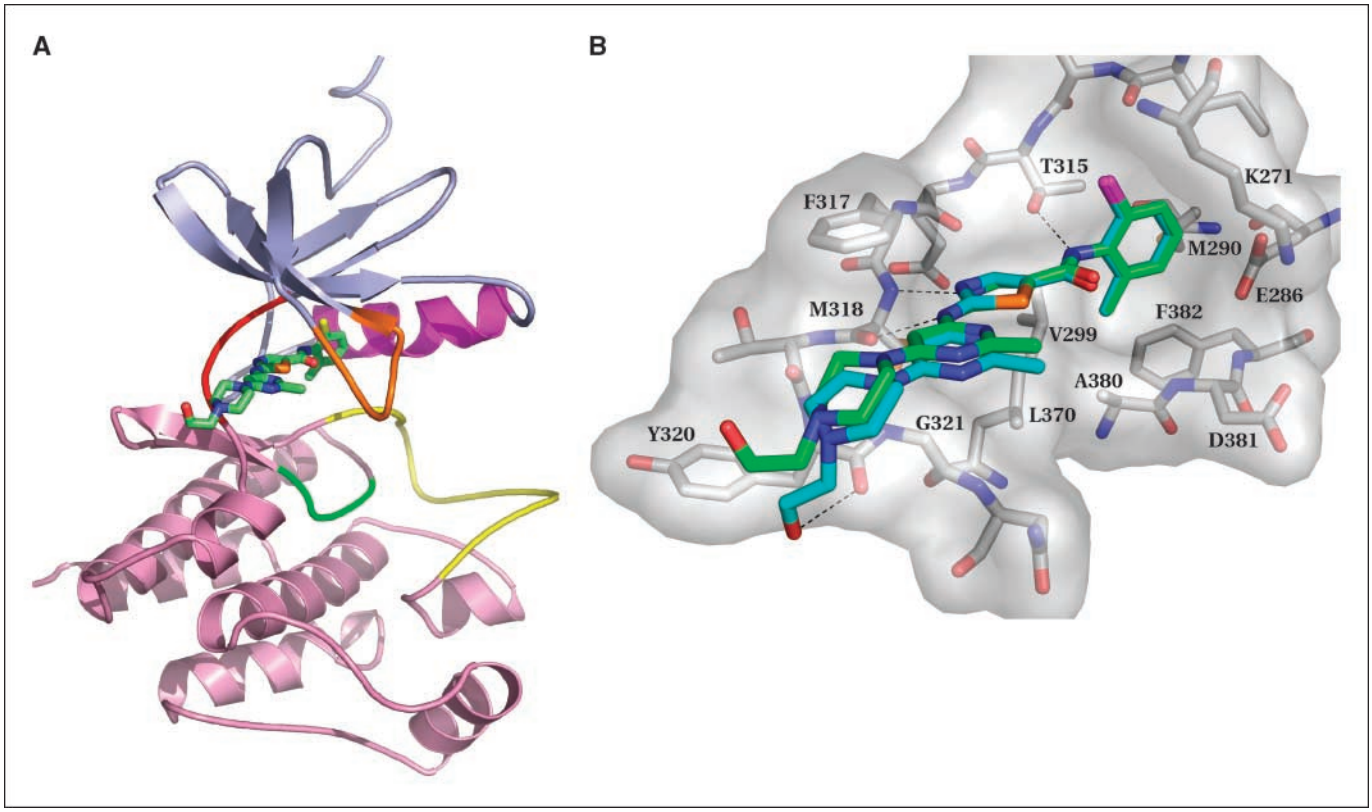


**Figure 2.** Structure of dasatinib complex. *A,* overview of the three-dimensional structure of ABL kinase with dasatinib. *Stick,* dasatinib; *green,* carbon atoms. *Blue,* $NH_2$-terminal lobe of ABL kinase; *orange,* P-loop; *magenta,* helix α-C; *red,* hinge region; *pink,* COOH-terminal lobe; *green,* catalytic loop; *yellow,* activation loop. *B,* cut-away detailed view of dasatinib and nearby residues in the ATP-binding site. *Green* and *blue,* inhibitor molecules found in the two asymmetric units; *gray,* one protein structure with surface of residues displayed. *Dashed lines,* hydrogen bonds.

**Cocrystallization of ABL inhibitor complexes.** All crystallization trials were by hanging-drop, vapor-diffusion method at 4°C. Equal volumes of protein inhibitor and reservoir solutions were mixed to form 2 μL drops. Cocrystals of ABL-dasatinib and ABL-imatinib could be grown spontaneously based on reported conditions (12), but the initial crystals of neither complex produced useful diffraction. Attempts to improve crystal quality by using crushed ABL-dasatinib crystals as microseeds were unsuccessful. In contrast, larger, separated, and more regularly shaped crystals of the ABL-imatinib complex were produced by streak microseeding (using a cat whisker) crushed ABL-imatinib crystals into fresh drops of 5 mg/mL ABL-imatinib mixed with reservoir solution from the initial hit. Seed-derived, ABL-imatinib crystals were crushed and used as microseeds to nucleate the growth of ABL-dasatinib crystals using the same procedure; diffraction quality crystals appeared in 3 days. The optimal reservoir solution was 22% (w/v) polyethylene glycol (PEG) 3350, 0.2 mol/L $MgSO_4$, and 0.1 mol/L MES (pH 6.5). Crystals were transferred by cryoloop into the cryoprotectant [30% (w/v) PEG 3350, 0.2 mol/L $MgSO_4$, and 0.1 mol/L MES (pH 6.5)] for 15 seconds and then relooped and flash cooled in liquid nitrogen.

**Structural determination and refinement.** Data collection was done at beamline X25 (National Synchrotron Light Source, Brookhaven National Laboratory, Upton, NY), with the wavelength tuned to 1.1 Å and equipped with a nitrogen cryostream set to 100 K and an ADSC Quantum 315 detector positioned at 240 mm (ADSC, Poway, CA). Diffraction images were processed with Denzo and Scalepack from the HKL suite (HKL, Charlottesville, VA; ref. 25). Intensities were converted to structure factor amplitudes and placed on an absolute scale with Truncate (26) from the CCP4 suite (27). Initial phases were calculated by molecular replacement by AMoRe (28), with the dimer from 1FPU used as the search model. The structure was refined with CNX (Accelrys, Inc., San Diego, CA; ref. 29) and modeled with Quanta (Accelrys). The data collection and refinement statistics are summarized in Table 1.

Although both the ABL-imatinib and the ABL-dasatinib cocrystals were rod shaped, they grew as different crystal forms. The dasatinib cocrystals belonged to space group $P4_32_12$, with unit cell dimensions of $a$ = 105.2 Å and $c$ = 111.1 Å, and contained two molecules per asymmetric unit. This crystal form differs from those of previously reported ABL kinase crystal structures (PDB IDs 1M52, 1IEP, 1FPU, 1OPJ, 1OPK, and 1OPL; refs. 12, 23, 30). This change in crystal form was unexpected because cocrystals of the imatinib complex, which came from the same tray as those used as seeds, were shown to be of the same form as 1IEP and 1FPU (space group F222 with unit cell dimensions of $a$ = 111.9 Å, $b$ = 146.8 Å, and $c$ = 152.9 Å and contained two molecules per asymmetric unit). The structure was determined by molecular replacement with the 1FPU dimer used as the search model. A solution was not found when one monomer from 1FPU was used as the search model presumably because the noncrystallographic 2-fold rotation axis, which is nearly parallel with the X axis at approximately $z$ = 3/8 and $y$ = 1/2, is closely aligned with one of the crystallographic 2-fold screw axes. Instead, the dimer from 1FPU was used, although, in hindsight, the dimer from 1M52 would have been the better choice based on structural homology.

**Coordinates.** The refined coordinates and structure factors were deposited in the PDB (31) as ID 2GQG.

## Results

**Structure of ABL-dasatinib complex.** We report the X-ray crystal structure of the human ABL kinase domain (residues 225-512) complexed with dasatinib at 2.4 Å resolution (Fig. 2*A*). The structure encompasses the main structural features of a typical protein kinase in the activated state. The protein kinase fold is separated into two subdomains or lobes. The smaller $NH_2$-terminal lobe is composed of a five-stranded β sheet and one prominent α

helix called helix α-C. The COOH-terminal lobe is larger than the $NH_2$-terminal lobe and is predominantly helical. The two lobes are connected through a single polypeptide strand (the linker/hinge region) that acts as a hinge about which the two domains can rotate with respect to one another on binding of ATP and/or substrate. The ATP-binding site is a deep cleft between the two lobes and sits beneath a highly flexible P-loop connecting strands β1 and β2. The P-loop contains a conserved glycine-rich sequence motif (GXGXφG), where φ, usually tyrosine or phenylalanine, caps the site of phosphate transfer. In ABL kinase, this residue is $Tyr^{253}$. The structure reveals that the P-loop is partially disordered, as indicated by high B-factors and broken electron density.

Dasatinib sits in the ATP site enveloped by the two lobes, with the aminothiazole moiety of the molecule occupying the site normally bound by the adenine group of ATP (Fig. 2*B*). The 2-chloro-6-methyl phenyl ring of dasatinib is orthogonal to the thiazole carboxamide group and probes into a mostly hydrophobic pocket near $Thr^{315}$ that is not occupied by ATP. The piperazine group points toward the surface-exposed portion of the hinge region. Three notable hydrogen bonds are identified between dasatinib and ABL. A pair of hydrogen bonds is formed in the hinge region of the ATP-binding site (i.e., between the 3-nitrogen of the aminothiazole ring of dasatinib and the amide nitrogen of $Met^{318}$ and between the 2-amino hydrogen of dasatinib with the carbonyl oxygen of $Met^{318}$). A hydrogen bond is also formed between the side chain hydroxyl oxygen of $Thr^{315}$ and the amide nitrogen of dasatinib. Dasatinib also participates in two heteroaromatic CH···O=C interactions with the hinge region backbone (i.e., the C4 thiazole carbon with the carbonyl oxygen of $Glu^{316}$ and the C5 pyrimidine carbon with the carbonyl oxygen of $Met^{318}$). These types of interactions have also been observed with other kinase inhibitor complexes (32, 33). Other contacts are mainly van der Waals interactions, including that of the substituted pyrimidine, which occupies a hydrophobic cleft created by $Leu^{248}$ and $Gly^{321}$, and that of the 2-chloro-6-methyl phenyl ring, which occupies a hydrophobic pocket composed of the $Thr^{315}$ methyl group, $Met^{290}$, $Val^{299}$, $Ile^{313}$, and $Ala^{380}$. The piperazine group rests on the surface-exposed COOH-terminal portion of the hinge region via van der Waals contacts. The terminal hydroxyethyl group interacts with protein in one of the two complexes in the asymmetric unit via a hydrogen bond between the hydroxyethyl group and the backbone carbonyl of $Tyr^{320}$. In the other complex, the hydroxyethyl group points in the opposite direction and is solvent exposed, indicating that this group may be highly mobile.

A comparison of the two ABL molecules in the asymmetric unit reveals that their overall conformation is nearly identical. The activation loop in both molecules is extended away from the ATP-binding site, as is observed in activated kinases. The activation loop not only provides the binding platform for peptide substrate interactions but also ensures the appropriate orientation of the catalytic machinery by virtue of the extended or "active" conformation. Phosphorylation of the activation loop is believed to stabilize the extended or active conformation and/or destabilize the folded or inhibitory conformation. An α-carbon backbone structural alignment of the kinase domain of both molecules of ABL and the activated SRC family member LCK (PDB ID 3LCK; ref. 34) reveals that, with the exception of the P-loop, which is flexible, both ABL molecules in the asymmetric unit adopt very similar conformations to activated LCK (Fig. 3*A*). $Tyr^{393}$ of the activation loop (the site of activating phosphorylation for wild-type ABL kinase) aligns well with its counterpart, phosphorylated $Tyr^{394}$ of LCK. Evidence for partial phosphorylation of $Tyr^{393}$ was observed, which is consistent with the forms of ABL kinase that were observed by mass spectrometry (MS; data not shown), and in fact one of the two ABL molecules in the asymmetric unit is phosphorylated at $Tyr^{393}$ (Fig. 3*B*). Interestingly, despite the differences in phosphorylation state, the position and conformation of $Tyr^{393}$ is similar between the two ABL molecules. The phosphorylated $Tyr^{393}$ makes a hydrogen bond with the side chain of $Arg^{386}$, whereas, in the unphosphorylated molecule, $Tyr^{393}$ is not involved in hydrogen bonding. Instead, the unphosphorylated $Tyr^{393}$ stacks with the hydrocarbon portion of the side chain of $Arg^{386}$, which makes a hydrogen bond via its guanidinium group with the backbone carbonyl of $Ser^{385}$.

Because the conformations are similar between the two ABL molecules in the unit cell, the following discussions will refer only to the phosphorylated molecule. The kinase-conserved "DFG" motif, $Asp^{381}$-$Phe^{382}$-$Gly^{383}$ (ABL numbering), which marks the $NH_2$-terminal portion of the activation loop, is seen to adopt the same conformation as that found in the activated LCK structure. Optimal phosphate transfer requires the precise spatial arrangement of several catalytic residues that are conserved among all tyrosine kinases, including $Asp^{363}$ and $Asn^{368}$, which emanate from the catalytic loop. $Asp^{363}$, the catalytic base, interacts with the

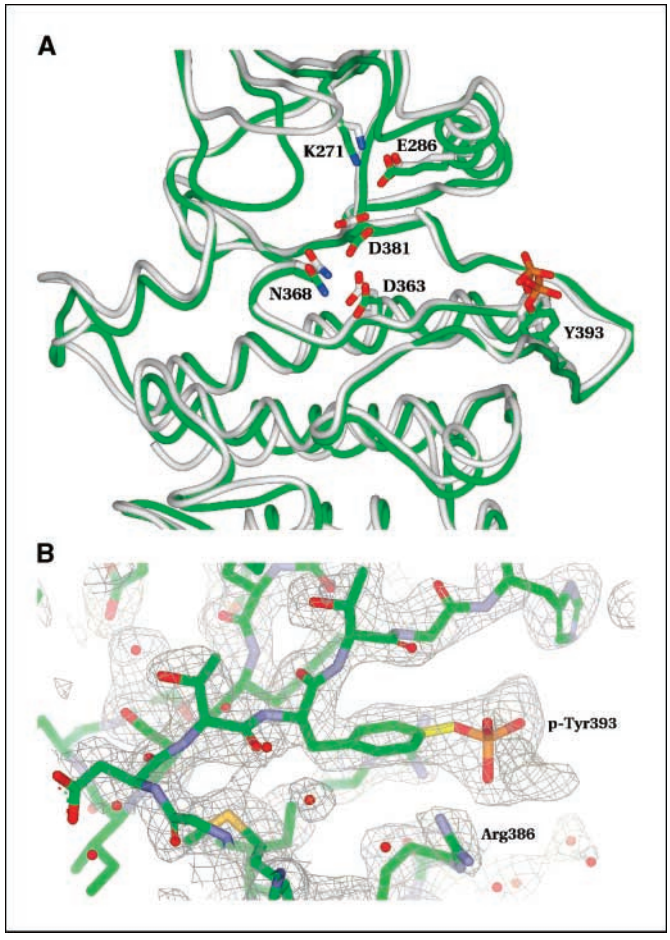


**Figure 3.** Comparison of dasatinib complex with an activated kinase. *A,* structure of ABL kinase (*green*) overlayed with LCK kinase (*gray*), (PDB ID 3LCK). Residues important for the catalytic machinery of a typical kinase. *B,* electron density of phosphorylated Y393 and nearby residues and waters.

attacking hydroxyl group of the substrate, whereas Asn$^{368}$ engages in hydrogen bonding interactions that orient Asp$^{363}$. Asp$^{381}$ of the DFG motif and Asn$^{368}$ are also required for the binding of two divalent metal cations involved in coordination of the triphosphate group. All of these residues in the ABL-dasatinib structure superimpose well with the activated LCK structure. It is also observed that a conserved Lys-Glu (Lys$^{271}$-Glu$^{286}$) salt bridge, important for maintaining an active kinase conformation and orienting the lysine side chain for interaction with the ATP phosphates, is present and similarly arranged as in the LCK structure. Collectively, the above observations indicate that dasatinib can bind to the activated form of ABL kinase.

**Structural comparison with other bound forms of ABL.** To provide a structural explanation for the greater potency of dasatinib versus imatinib against BCR-ABL, structural comparisons were made between ABL-dasatinib and other bound forms of the enzyme. First, a structural comparison of the ABL-dasatinib complex was made with the imatinib-bound form of ABL (PDB ID 1IEP; ref. 12). Imatinib has been shown previously to bind to BCR-ABL only when the enzyme is in its inactive conformation (12, 23). The most striking difference between the two ABL structures is the conformation of the activation loop (Fig. 4). The activation loop in the imatinib-bound form folds back toward the ATP-binding site, forming interactions with both the P-loop and the inhibitor, thus resulting in an inhibitory kinase conformation. The differences in the activation loop conformation between the two forms of ABL begin at the DFG motif. Phe$^{382}$ of the DFG motif in the imatinib-bound form points toward the ATP-binding site, π-stacks with the pyrimidine ring of imatinib and forms an edge-to-face interaction with Tyr$^{253}$ of the P-loop. In contrast, in the dasatinib-bound form, Phe$^{382}$ is buried in a hydrophobic pocket not accessed by ATP, as is typically found with activated kinases (Fig. 2*B*). Although the central cores of dasatinib and imatinib overlap, the rest of the structures extends in opposite directions within the protein. Specifically, the *N*-2-hydroxyethylpiperidine group of dasatinib, for which there is no imatinib counterpart, extends out toward solvent-exposed protein. Conversely, dasatinib does not protrude toward the hydrophobic pocket occupied by Phe$^{382}$, as does the benzamidine branch of imatinib. The latter observation shows why the activation loop is able to exist in the active conformation in the presence of bound dasatinib but not in the presence of bound imatinib (Fig. 4). The P-loop bends toward imatinib to form close interactions with the kinase inhibitor, including an edge-to-face aromatic interaction between Tyr$^{253}$ and the pyridine and pyrimidine rings. Compared with the imatinib-bound form, the P-loop in the dasatinib-bound structure is more extended, although the electron density was weak for this part of the protein. The hydroxyl moiety of Tyr$^{253}$ seems to engage in a hydrogen bond with the backbone carbonyl of Arg$^{367}$ in the ABL-dasatinib structure.

The dasatinib-bound structure of ABL was also compared with the PD173955-bound form of ABL (PDB ID 1M52; ref. 12). The structural comparison reveals that dasatinib occupies a similar portion of the ATP-binding site of ABL, as does PD173955. However, the *N*-2-hydroxyethylpiperidine group of dasatinib extends further out toward solvent-exposed protein compared with PD173955. The activation loop in the PD173955-bound form is extended, but the DFG motif is not found in the proper catalytic orientation as it is in the dasatinib-bound form. Beginning at Asp$^{381}$, the DFG residues are observed to kink in opposite directions between the two structures, such that PD173955-bound Phe$^{382}$ and Asp$^{381}$ occupy the corresponding positions of dasatinib-bound Asp$^{381}$ and Phe$^{382}$, respectively. The P-loop in the PD173955-bound form also adopts a different conformation and is observed to bend further in toward the ATP-binding site than the P-loop in the dasatinib-bound form.

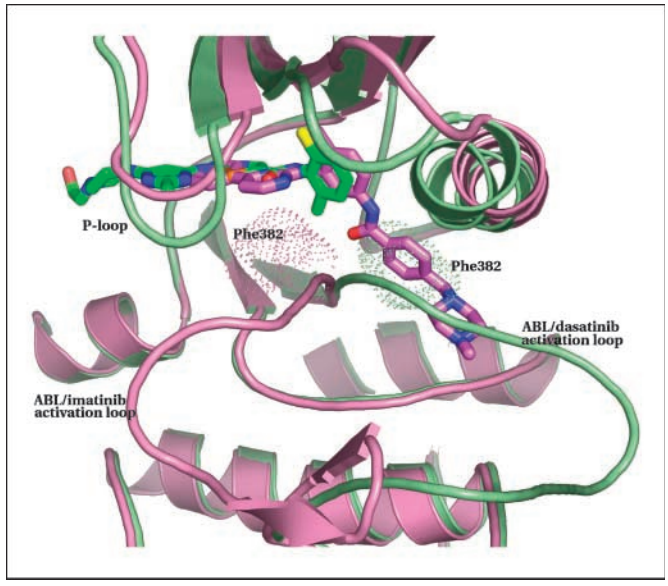


**Figure 4.** A comparison of dasatinib complex with imatinib complex. A ribbon representation of the ABL-dasatinib complex (protein and dasatinib carbons, *green*) overlayed with the corresponding complex of ABL-imatinib (protein and imatinib carbons, *purple*). The activation loops are labeled. Note the diverging direction of the activation loop in the two structures. Phe$^{382}$ of the DFG motif (activation loop) in a dot surface representation for each complex to show that imatinib would not be able to bind to the active conformation of ABL because of a clash with Phe$^{382}$ (as well as other activation loop residues) as found in the dasatinib-bound ABL conformation. Dasatinib, on the other hand, would be able to bind to the imatinib-bound activation loop conformation.

Based on modeling of dasatinib in the imatinib-bound and the PD173955-bound forms of ABL, there do not seem to be any major steric clashes that would preclude dasatinib from also binding to the inactive conformations found in these other ABL structures. However, a few unfavorable intermolecular contacts would exist with a small portion of the P-loop in each of the other ABL structures. This is most likely because the P-loop contorts to allow Tyr$^{253}$ to interact with imatinib and PD173955 (and also with Phe$^{382}$ of the activation loop), whereas Tyr$^{253}$ is not seen to interact with dasatinib in our structure. The P-loop is very flexible, and so with minor movement of the P-loop away from the PD173955-bound and imatinib-bound positions, it seems that dasatinib can also bind to these forms. Because the electron density of the P-loop of our structure is not very definitive, one would speculate that the P-loop is mobile even when dasatinib is bound, indicating that, for the most part, it is not forming a critical interaction. The lack of P-loop interactions by dasatinib may actually be advantageous because several imatinib-resistant ABL mutations appear in the P-loop. The above observations suggest that the increased wild-type ABL binding affinity of dasatinib over imatinib is at least partially due to the apparent ability of dasatinib to recognize multiple states of the enzyme.

**Structural basis for activity against imatinib-resistant ABL mutations.** The activity of dasatinib was previously assessed against 15 clinically relevant imatinib-resistant BCR-ABL mutants covering 12 different amino acid locations (M244V, G250E, Q252H/R, Y253F/H, E255K/V, T315I, F317L, M351T, E355G, F359V, H396R, and F486S; ref. 16). Several imatinib-resistant mutation sites are in

contact with imatinib, whereas others are speculated to be involved in stabilization of the specific inactive imatinib-bound conformation of ABL. Only the T315I mutant was clearly resistant to dasatinib, retaining kinase activity even in the presence of micromolar concentrations of the compound. The only other mutant showing any appreciable decrease in sensitivity was the F317L mutant, which required ~3- to 5-fold higher concentrations of dasatinib to inhibit the growth of Ba/F3 cells. Interestingly, the Q252R mutant was consistently more sensitive to dasatinib compared with wild-type BCR-ABL.

The activity profile of dasatinib against the 15 imatinib-resistant BCR-ABL mutants is, for the most part, remarkably consistent with insight gained from an examination of the amino acid locations of the mutants in the crystal structure of ABL kinase with dasatinib (Fig. 5). Dasatinib is involved in a hydrogen bond with the side chain of T315, and the side chain methyl group of this amino acid residue is involved in van der Waals contact with the 2-chloro-6-methyl phenyl ring. As such, T315 is a critical contact residue for dasatinib. The resistance of the T315I mutant is most likely due to the loss of a hydrogen bond and increased steric bulk in this pocket. F317 was observed to make off-center aromatic π-stacking with the pyrimidine and thiazole rings of dasatinib, which may explain the slight loss in activity of dasatinib against the F317L mutant.

The difference in P-loop conformation between the dasatinib- and imatinib-bound forms of ABL can help explain the difference in activity between the two inhibitors against the M244V, G250E, Q252H/R, Y253F/H, and E255K/V mutants. A G250E mutation might be expected to reduce flexibility of the P-loop, thereby not allowing the P-loop to adopt the imatinib-induced conformation. The improved activity of dasatinib against the G250E mutant may result from the fact that P-loop interactions seem less important for dasatinib. Q252 points into solvent in the dasatinib-bound form of ABL, explaining why the Q252H/R mutants are not resistant to dasatinib, but it is unclear from the structure why the Q252R mutant would be more sensitive to dasatinib compared with wild-type BCR-ABL. In the imatinib-bound form, however, the side chain of Q252 contributes to the distorted P-loop conformation by packing up against Y253, which in turn interacts with imatinib and hydrogen bonds with N322. Y253 does not interact with dasatinib, but the hydroxyl of Y253 is seen to hydrogen bond with the backbone of R367, an interaction that must not be critical due to the maintenance of dasatinib activity against the Y253F mutant. E255 hydrogen bonds to its own backbone in the dasatinib-bound form, whereas, in the imatinib-bound form, it hydrogen bonds with the hydroxyl of Y257, stabilizing the imatinib-bound conformation of the P-loop. M244 is proximal to, and makes contacts with, the P-loop in both the dasatinib-bound and the imatinib-bound forms of ABL. Changes in the identity of this residue most likely result in changes in its interactions with the P-loop, potentially destabilizing the specific inactive ABL conformation that is a prerequisite for imatinib binding.

The conformation of H396, which resides in the activation loop, is slightly different between the two ABL molecules in the asymmetric unit cell of the dasatinib-bound form. In either molecule, there are no discernable interactions of this residue with protein or inhibitor, which may explain why the H396R mutation does not affect dasatinib activity. H396 in the imatinib-bound form, however, is involved in a hydrogen bond that stabilizes the inactive conformation of the activation loop. The position and conformation of the other COOH-terminal lobe mutation site residues, M351, E355, F359, and F486, are similar between the dasatinib- and imatinib-bound forms of ABL. However, it is postulated that these residues, which neighbor the activation loop, are critical for maintaining the particular inactive imatinib-bound conformation. F359 is also involved in van der Waals contacts with both imatinib and the activation loop in the imatinib-bound form. Dasatinib does not reside near this residue, explaining its potency against BCR-ABL with mutations at this site.

## Discussion

The results of this study provide the first view of the catalytic domain of wild-type ABL kinase in an active conformation, wherein the entire catalytic machinery is in the proper orientation and $Tyr^{393}$ is phosphorylated. Our structure also provides insight into the molecular mechanism of inhibition of ABL kinase by dasatinib, which binds in the ATP-binding site and presumably displaces ATP. The observation that ABL can adopt the same active conformation independent of activation loop phosphorylation at $Tyr^{393}$ may indicate that this conformation is inherently stable. The fact that the catalytic activity of the isolated ABL kinase domain, in the absence of regulatory domains, is not increased significantly by phosphorylation in the activation loop supports this notion (23). Based on modeling of dasatinib in other conformations of ABL, we suggest that the greater ABL binding affinity of dasatinib over imatinib is at least partially due to the apparent ability of dasatinib to recognize multiple states of the enzyme.

Our X-ray analysis also sheds light on the favorable activity of dasatinib against clinically relevant imatinib-resistant BCR-ABL mutants (16). Several imatinib-resistant BCR-ABL mutants occur in the P-loop, which adopts a distorted conformation in the imatinib-bound form of ABL to make critical contacts with the inhibitor and

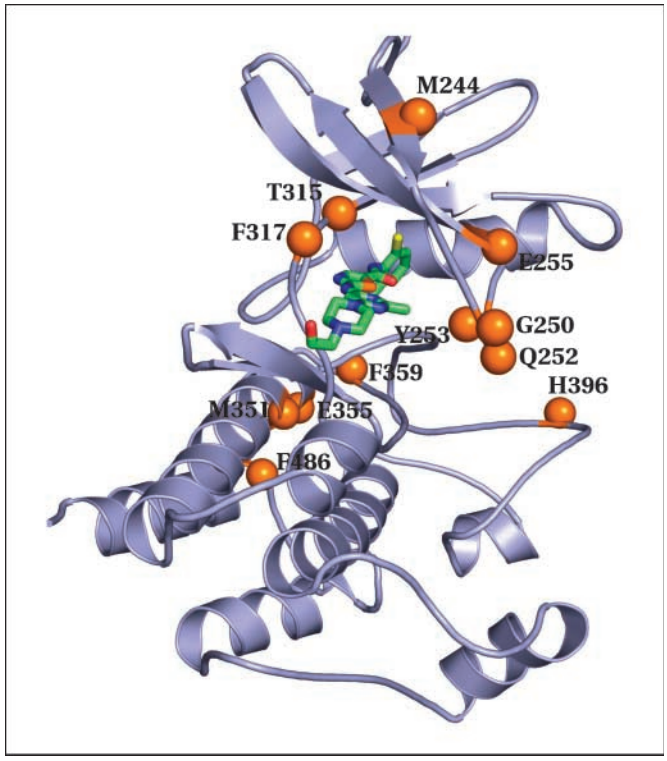


**Figure 5.** The position of the imatinib-resistant mutation sites are mapped onto the ABL-dasatinib complex structure. *Orange spheres,* C-α atoms.

the activation loop. Based on our structure, P-loop interactions do not seem to be as important for dasatinib binding to ABL. Several residues at the other mutation sites are speculated to be also involved in stabilization of the specific inactive imatinib-bound conformation of ABL. The observation that ABL conformational requirements are less stringent for dasatinib than for imatinib and that dasatinib is not involved in critical interactions with many of the mutated residues further explains the positive activity profile of dasatinib. The structure also reveals that a critical interaction is made directly between dasatinib and $Thr^{315}$ of the hinge region and explains the loss of activity against the T315I mutant.

This structure provides further experimental evidence that the activation loop of a kinase can, in general, adopt multiple conformations (35–37). Phosphorylation of the activation loop is believed to stabilize the extended or active conformation and/or destabilize the folded or inhibitory conformation(s), of which there could be many. If the etiology of many cancers involves the aberrant activation of kinases, then one may postulate that inhibiting the active kinase conformation may produce a more favorable outcome than inhibition that is dependent on an inactive kinase conformation. More evidence is needed to determine whether inhibiting multiple forms, only the activated form or only a particular inactive conformation of ABL, will result in superior inhibition, *in vivo* potency, and/or specificity. Some native kinases, such as KIT, exist in an autoinhibitory state due to the activation loop inserting into the kinase active site, thus disrupting formation of the activated structure (38). Interestingly, imatinib, a potent KIT inhibitor and now the standard frontline therapy for advanced gastrointestinal stromal tumors (39, 40) binds to an inactive conformation of KIT (38). However, most KIT activation loop mutations are resistant to clinically achievable doses of imatinib (41, 42), which can be explained by the findings that KIT activation loop mutations not only activate kinase activity but also stabilize the activation loop in a conformation that does not allow productive imatinib binding (38, 43). Dasatinib has recently been shown to be a potent inhibitor of wild-type KIT and imatinib-resistant KIT activation loop mutants (44), providing another example where an inhibitor that requires less stringent conformational requirements retains activity and where mutations that affect specific conformations may consequently alter the potency of inhibitors targeting these specific states. Dasatinib should contribute valuable information as it progresses through the clinic on the effectiveness of a drug not limited to the binding of one particular state.

Preclinical and clinical data obtained to date suggest that, for human leukemia that is driven by BCR-ABL, the apparent ability of dasatinib to bind to both the active and the inactive conformations of BCR-ABL affords this agent greater therapeutic potential compared with an agent, such as imatinib, which binds only to an inactive form of the enzyme. Phase I and II clinical experience has shown promising results for dasatinib in patients with imatinib-resistant and imatinib-intolerant disease (18–22). The lack of cross-resistance between dasatinib and imatinib, as evidenced by dasatinib retaining inhibitory activity against multiple imatinib-resistant forms of BCR-ABL *in vitro*, may result in dasatinib producing greater durability of response. Further follow-up of the phase II trials is awaited with interest.

In conclusion, the current study reveals that the potency and favorable profile of dasatinib against wild-type ABL and imatinib-resistant ABL mutants is at least partially due to its ability to recognize multiple states of BCR-ABL. Our findings highlight the importance of considering kinase enzyme conformation in the rational design of kinase inhibitors for cancer targets.

## Acknowledgments

Received 11/28/2005; revised 2/8/2006; accepted 3/23/2006.

**Grant support:** Offices of Biological and Environmental Research of the Offices of Basic Energy Sciences of the U.S. Department of Energy and the National Center of Research Resources of the NIH.

The costs of publication of this article were defrayed in part by the payment of page charges. This article must therefore be hereby marked *advertisement* in accordance with 18 U.S.C. Section 1734 solely to indicate this fact.

We thank Dr. Michael Becker (Department of Biology, Brookhaven National Laboratory) for preparing beamline X25 at the National Synchrotron Light Source for data collection and Bethanne Warrack (Bristol-Myers Squibb, Princeton, NJ) for MS analysis of ABL kinase.

## References

1. Sawyers CL. Chronic myeloid leukemia. N Eng J Med 1999;340:1330–40.
2. Daley GQ, Van Etten RA, Baltimore D. Induction of chronic myelogenous leukaemia in mice by the P210 bcr/abl gene of the Philadelphia chromosome. Science 1990;247:824–30.
3. Faderl S, Kantarjian HM, Thomas DA, et al. Outcome of Philadelphia chromosome-positive adult acute lymphoblastic leukemia. Leuk Lymphoma 2000;36:263–73.
4. Melo JV, Hughes TP, Apperley JF. Chronic myeloid leukemia. Hematology (Am Soc Hematol Educ Program) 2003;132–52.
5. Druker BJ, Talpaz M, Resta DJ, et al. Efficacy and safety of a specific inhibitor of the BCR-ABL tyrosine kinase in chronic myeloid leukemia. N Engl J Med 2001;344:1031–7.
6. Druker BJ, Sawyers CL, Kantarjian H, et al. Activity of a specific inhibitor of the BCR-ABL tyrosine kinase in the blast crisis of chronic myeloid leukemia and acute lymphoblastic leukemia with the Philadelphia chromosome. N Eng J Med 2001;344:1038–42.
7. Ottmann OG, Druker BJ, Sawyers CL, et al. A phase 2 study of imatinib in patients with relapsed or refractory Philadelphia chromosome-positive acute lymphoid leukemias. Blood 2002;100:1965–71.
8. Talpaz M, Silver RT, Druker BJ, et al. Imatinib induces durable hematologic and cytogenetic responses in patients with accelerated phase chronic myeloid leukemia: results of a phase 2 study. Blood 2002;99:1928–37.
9. Gorre ME, Mohammed M, Ellwood K, et al. Clinical resistance to STI-571 cancer therapy caused by BCR-ABL gene mutation or amplification. Science 2001;293:876–80.
10. Donato NJ, Wu JY, Stapley J, et al. BCR-ABL independence and LYN kinase overexpression in chronic myelogenous leukemia cells selected for resistance to STI571. Blood 2003;101:690–8.
11. Shah NP, Nicoll JM, Nagar B, et al. Multiple BCR-ABL kinase domain mutations confer polyclonal resistance to the tyrosine kinase inhibitor imatinib (STI571) in chronic phase and blast crisis chronic myeloid leukemia. Cancer Cell 2002;2:117–25.
12. Nagar B, Bornmann WG, Pellicena P, et al. Crystal structures of the kinase domain of c-Abl in complex with the small molecule inhibitors PD173955 and imatinib (STI-571). Cancer Res 2002;62:4236–43.
13. Azam M, Latek RR, Daley GQ. Mechanisms of autoinhibition and STI-571/imatinib resistance revealed by mutagenesis of BCR-ABL. Cell 2003;112:831–43.
14. Lombardo LJ, Lee FY, Chen P, et al. Discovery of *N*-(2-chloro-6-methylphenyl)-2-(6-(4-(2-hydroxyethyl) piperazin-1-yl)-2-methylpyrimidin-4-ylamino)thiazole-5-carboxamide (BMS-54825), a dual Src/Abl kinase inhibitor with potent antitumor activity in preclinical assays. J Med Chem 2004;47:6658–61.
15. O'Hare T, Walters DK, Stoffregen EP, et al. *In vitro* activity of Bcr-Abl inhibitors AMN107 and BMS-354825 against clinically relevant imatinib-resistant Abl kinase domain mutants. Cancer Res 2005;5:4500–5.
16. Shah NP, Tran C, Lee FY, Chen P, Norris D, Sawyers CL. Overriding imatinib resistance with a novel ABL kinase inhibitor. Science 2004;305:399–401.
17. Branford S, Rudzki Z, Walsh S, et al. Detection of BCR-ABL mutations in patients with CML treated with imatinib is virtually always accompanied by clinical resistance, and mutations in the ATP phosphate-binding loop (P-loop) are associated with a poor prognosis. Blood 2003;102:276–83.
18. Sawyers CL, Kantarjian HM, Shah NP, et al. Dasatinib (BMS-354825) in patients with chronic myeloid leukemia (CML) and Philadelphia-chromosome positive acute lymphoblastic leukemia (Ph+ ALL) who are resistant or intolerant to imatinib: update of a phase I study [abstract 38]. Blood 2005;106:16a.
19. Guilhot F, Apperley JF, Shah NP, et al. A phase II study of dasatinib in patients with accelerated phase chronic myeloid leukemia (CML) who are resistant or intolerant to imatinib: first results of the CA180005 'START-A' study [abstract 39]. Blood 2005;106:16a.
20. Talpaz M, Rousselot P, Kim DW, et al. A phase II study of dasatinib in patients with chronic myeloid leukemia (CML) in myeloid blast crisis who are resistant or intolerant to imatinib: first results of the CA180006 'START-B' study [abstract 40]. Blood 2005;106:16a.
21. Hochhaus A, Baccarani M, Sawyers C, et al. Efficacy of dasatinib in patients with chronic phase Philadelphia chromosome-positive CML resistant or intolerant to imatinib: first results of the CA180013 'START-C' phase II study [abstract 41]. Blood 2005;106:17a.

22. Ottmann OG, Martinelli G, Dombret H, et al. A phase II study of dasatinib in patients with chronic myeloid leukemia (CML) in lymphoid blast crisis or Philadelphia-chromosome positive acute lymphoblastic leukemia (Ph+ ALL) who are resistant or intolerant to imatinib: the 'START-L' CA180015 study [abstract 42]. Blood 2005; 106:17a.
23. Schindler T, Bornmann W, Pellicena P, Miller WT, Clarkson B, Kuriyan J. Structural mechanism for STI-571 inhibition of abelson tyrosine kinase. Science 2000;289: 1938–42.
24. Weber W, Weber E, Geisse S, Memmert K. Optimisation of protein expression and establishment of the Wave Bioreactor for baculovirus/insect cell culture. Cytotechnology 2002;38:77–85.
25. Otwinowski Z, Minor W. Processing of X-ray diffraction data collected in oscillation mode. Methods Enzymol 1997;276:307–26.
26. French S, Wilson K. On the treatment of negative intensity observations. Acta Crystallogr A 1978;34:517–25.
27. Bailey S. The CCP4 suite: programs for protein crystallography. Acta Crystallogr D Biol Crystallogr 1994;50 Pt 5:760–3.
28. Navaza J. AMoRe: an automated package for molecular replacement. Acta Crystallogr A 1994;50: 157–63.
29. Brünger AT, Adams PD, Clore GM, et al. Crystallography & NMR system: a new software suite for macromolecular structure determination. Acta Crystallogr D Biol Crystallogr 1998;54 Pt 5:905–21.
30. Nagar B, Hantschel O, Young MA. Structural basis for the autoinhibition of c-Abl tyrosine kinase. Cell 2003; 112:859–71.
31. Berman HM, Westbrook J, Feng Z. The Protein Data Bank. Nucleic Acids Res 2000;28:235–42.
32. Kim KS, Kimball SD, Misra RN, et al. Discovery of aminothiazole inhibitors of cyclin-dependent kinase 2: synthesis, X-ray crystallographic analysis, and biological activities. J Med Chem 2002;45:3905–27.
33. Pierce AC, Sandretto KL, Bemis GW. Kinase inhibitors and the case for CHO hydrogen bonds in protein-ligand binding. Proteins 2002;49:567–76.
34. Yamaguchi H, Hendrickson WA. Structural basis for activation of human lymphocyte kinase Lck upon tyrosine phosphorylation. Nature 1996;384:484–9.
35. Johnson LN, Noble MEM, Owen DJ. Active and inactive protein kinases: structural basis for regulation. Cell 1996;85:149–58.
36. Huse M, Kuriyan J. The conformational plasticity of protein kinases. Cell 2002;109:275–83.
37. Nolen B, Taylor S, Ghosh G. Regulation of protein kinases: controlling activity through activation segment conformation. Mol Cell 2004;15:661–75.
38. Mol CD, Dougan DR, Schneider TR, et al. Structural basis for the autoinhibition and STI-571 inhibition of c-Kit tyrosine kinase. J Biol Chem 2004;279:31655–63.
39. Heinrich M, Griffith D, Druker B, Wait C, Ott K, Zigler A. Inhibition of c-kit receptor tyrosine kinase activity by STI 571, a selective tyrosine kinase inhibitor. Blood 2000; 96:925–32.
40. Corless C, Fletcher J, Heinrich M. Biology of gastrointestinal stromal tumors. J Clin Oncol 2004;22: 3813–25.
41. Ma Y, Zeng S, Metcalfe D. The c-KIT mutation causing human mastocytosis is resistant to STI571 and other KIT kinase inhibitors; kinases with enzymatic site mutations show different inhibitor sensitivity profiles than wild-type kinases and those with regulatory-type mutations. Blood 2002;99:1741–4.
42. Frost M, Ferrao P, Hughes T, Ashman L. Juxtamembrane mutant V560GKit is more sensitive to imatinib (STI571) compared with wild-type c-kit whereas the kinase domain mutant D816VKit is resistant. Mol Cancer Ther 2002;1:1115–24.
43. Foster R, Griffith R, Ferrao P, Ashman L. Molecular basis of the constitutive activity and STI571 resistance of Asp816Val mutant KIT receptor tyrosine kinase. J Mol Graph Model 2004;23:139–52.
44. Schittenhelm MM, Shiraga S, Schroeder A, et al. Dasatinib (BMS-354825), a dual SRC/ABL kinase inhibitor, inhibits the kinase activity of wild-type, juxtamembrane, and activation loop mutant KIT isoforms associated with human malignancies. Cancer Res 2006; 66:473–81.